

Effect of View, Scan Orientation and Analysis Volume on Digital Tomosynthesis (DTS) Based Textural Analysis of Bone

WOONG KIM,^{1,3} DANIEL ORAVEC,¹ GEORGE W. DIVINE,² MICHAEL J. FLYNN,¹ and YENER N. YENI¹

¹Bone and Joint Center, Henry Ford Hospital, Integrative Biosciences Center (iBio), 6135 Woodward, Detroit, MI 48202, USA;

²Department of Public Health Science, Henry Ford Hospital, Detroit, MI, USA; and ³Cook Medical Inc., 1 Geddes Way, West Lafayette, IN, USA

(Received 28 July 2016; accepted 5 January 2017; published online 12 January 2017)

Associate Editor Sean S. Kohles oversaw the review of this article.

Abstract—Digital tomosynthesis (DTS) derived textural parameters of human vertebral cancellous bone have been previously correlated to the finite element (FE) stiffness and 3D microstructure. The objective of this study was to optimize scanning configuration and use of multiple image slices in the analysis, so that FE stiffness prediction using DTS could be maximized. Forty vertebrae (T6, T8, T11, and L3) from ten cadavers (63–90 years) were scanned using microCT to obtain trabecular bone volume fraction (BV/TV) and FE stiffness. The vertebrae were then scanned using DTS anteroposteriorly (AP) and laterally (LM) while aligned axially (0°), transversely (90°) or obliquely (23°) to the superior–inferior axis of the vertebrae. From the serial DTS images, fractal dimension (FD), mean intercept length (MIL) and line fraction deviation (LFD) parameters were obtained from a 2D-single mid-stack location and 3D-multi-image stack. The DTS derived textural parameters were then correlated with FE stiffness using linear regression models within each scanning orientation. 3D-multi-image stack models obtained from Transverse-LM scanning orientation (90°) were most explanatory regardless of accounting for the effects of BV/TV. Therefore, DTS scanning perpendicular to the axis of the spine in an LM view is the preferred configuration for prediction of vertebral cancellous bone stiffness.

Keywords—Vertebral cancellous bone, Large scale finite element modeling, Stiffness, Fractal dimension, Lacunarity, Mean intercept length, Line fraction deviation, Cadaver study.

INTRODUCTION

Osteoporosis and osteopenia is a widespread metabolic bone disease characterized by decreased bone mass and poor bone quality affecting 54 million U.S. adults age 50 and older.³⁵ Vertebral fractures are among the most common; one in every two elderly women is expected to have at least one vertebral fracture.²² Currently, bone mineral density (BMD) remains the most widely used measure of bone quality and fracture risk, but its ability to predict vertebral strength and fracture has been limited.^{3,18,19,26,30} Several *in vitro* studies have shown that significant improvements in prediction of bone strength can be made by addition of cancellous bone microstructural information into the fracture strength analysis.^{1,5,10,20,23,32} Clinically, however, access to the cancellous morphology or texture is limited by radiation dosage or available to extremities only.^{12,14,15,23,33}

Digital tomosynthesis (DTS) is a relatively new imaging modality that has a high in-plane resolution (150–300 μm), but about 1/5th the exposure of a CT exam, offering the possibility to examine vertebral bone microstructure within clinically acceptable radiation exposure levels (Fig. 1).^{6,7} Recently it was demonstrated that 2D textural parameters of human vertebral trabecular bone obtained from DTS can be used to predict 3D microstructure and finite element (FE) stiffness of the tissue.¹¹ In that study, DTS parameters were obtained from a single mid-coronal slice of the stack (out of 70 slices) that was acquired through anterior–posterior (AP) projection using a scan orientation in which the motion of the X-ray source–detector pair was transverse to the superior–inferior (SI) axis. However, the extent to which using a different scan and analysis configuration affects the examined relationships is unknown.

Address correspondence to Yener N. Yeni, Bone and Joint Center, Henry Ford Hospital, Integrative Biosciences Center (iBio), 6135 Woodward, Detroit, MI 48202, USA. Electronic mail: yeni@bjc.hfh.edu

The primary aim of the current study, thus, was to explore scan orientations parallel, transverse and oblique to the axis of the spine in combination with AP and lateral views, and using multiple DTS slices in the analysis in an attempt to identify scan and analysis conditions that offer maximum textural information to predict cancellous bone stiffness.

METHODS

Subjects and Specimens

Following institutional approval, forty cadaveric human vertebral bodies (T6, T8, T11, and L3) from five male (age range 75 ± 9.4 years) and five female (84 ± 4.6 years) were used. These donors were without medical history of infectious diseases (e.g., HIV, hepatitis), metabolic diseases known to affect bone (e.g., diabetes, kidney failure), corticosteroid usage, spinal surgery or a cause of death involving trauma.

Microcomputed Tomography (μ CT) and 3D-Stereological Analysis

All vertebrae were scanned and reconstructed at an isotropic voxel size of $45 \mu\text{m}$ using an in-house μ CT system previously described.^{11,29} The largest possible cubical volume of interest (VOI) consisting of only cancellous bone was cropped from the reconstructed images. The VOI was then segmented using an established global thresholding method and bone volume fraction (BV/TV) was calculated to be used as a covariate in the analysis.^{10,13,37}

Linear μ FE Modeling

Linear elastic FE models with isotropic element properties were constructed from the cubical VOI cropped out of the μ CT images and solved for uniaxial superior–inferior compression with “free-end” boundary conditions using custom software as described previously.^{10,37} Models were simulated once using heterogeneous tissue moduli where the modulus values were scaled with μ CT attenuation calibrated to a reference included in scans^{11,21} and once using a homogenous tissue modulus of 5 GPa. In both types of models, Poisson’s ratio was 0.3. Cancellous bone stiffness was calculated from the reaction forces and the uniaxial displacement for heterogeneous (E_v) and homogeneous (E_h) models.

Digital Tomosynthesis (DTS)

The same vertebral bodies were immersed in saline in a custom made radiologically transparent housing and scanned using DTS (Shimadzu Sonialvision Safire II) in a similar manner reported previously.¹¹ Six scanning configurations were employed (Fig. 2) using three scanning angles; vertebral bodies aligned axially (0°), transversely (90°) or obliquely (23°) to the SI axis, and two projection configurations; anterior–posterior (AP) and lateral–medial (LM). The 23° oblique orientation was included as a tradeoff between axial and transverse orientations as patients can be positioned diagonally on the scan table at this angle.

A cuboidal volume of interest (VOI) was cropped from each reconstructed DTS image-stack to include as much cancellous bone as possible (Fig. 3). The VOI was determined as the largest cuboid of cancellous

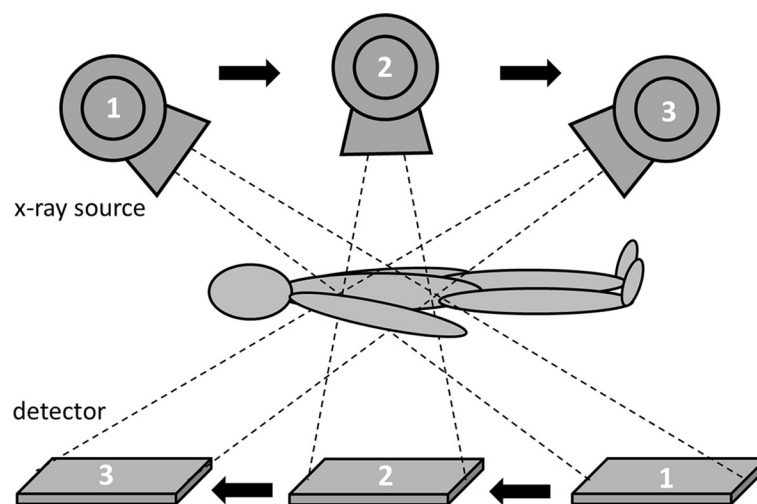


FIGURE 1. Schematic illustration of the DTS geometry. The X-ray source and the digital detector move in a parallel path in opposite directions acquiring a sequence of digital radiographs. Coronal (if AP view) or sagittal (if lateral view) slice images are reconstructed from projection images using filtered backprojection.

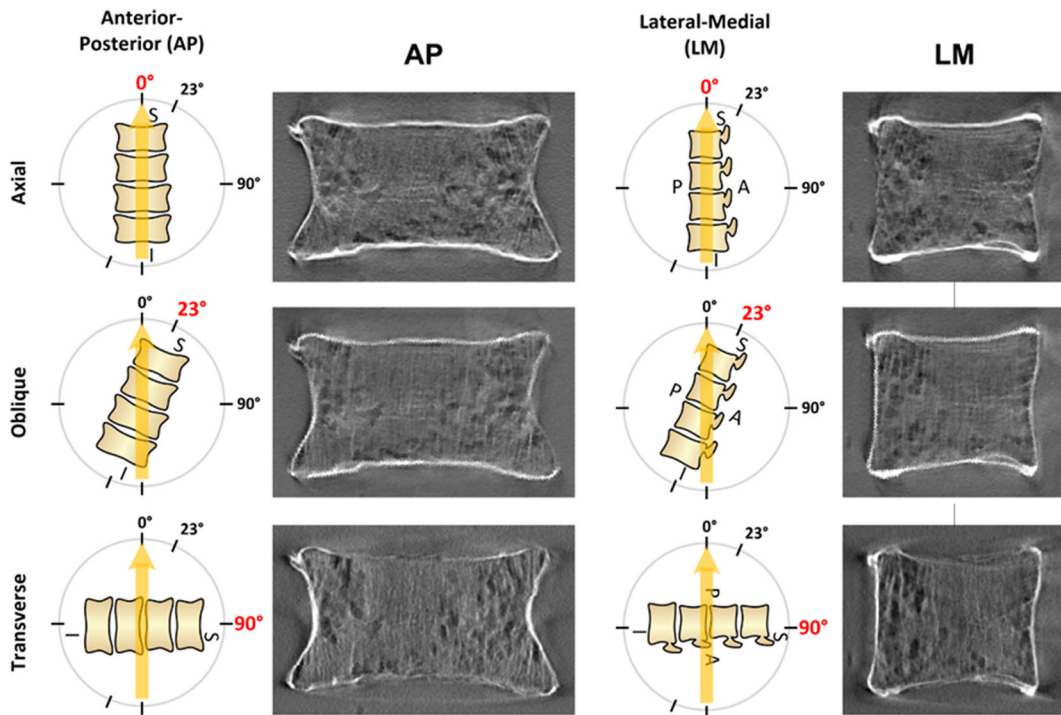


FIGURE 2. A set of coronal and sagittal slices from an L1 vertebra scanned at 0° (Axial), 23° (Oblique) and 90° (Transverse) to the spinal axis in AP (anterior–posterior) and LM (lateral–medial) views. The arrows show the orientation in which the source–detector pair moves in each scan configuration. Note the more prominent appearance of structures perpendicular to the scan orientation (e.g., endplates in axial and the shell in transverse scans).

volume excluding endplates and the vertebral shell for each vertebra. Each slice within the VOI was analyzed individually using fractal, mean intercept length (MIL)³⁴ and line fraction deviation (LFD)⁸ analyses. In the fractal analysis, fractal dimension (FD),⁴ mean lacunarity (λ) and the slope of lacunarity vs. box size relationship (S_λ) were calculated.²⁸ In MIL and LFD analyses, the mean (Av), standard deviation (SD), maximum (Max) and degree of anisotropy (DA, ratio of the principal measurements of MIL or LFD) were recorded for each slice (Fig. 3).

For each stack, average (Av) and standard deviation (SD) of FD, λ , S_λ , MIL.Max, MIL.Av, MIL.SD, MIL.DA, LFD.Max, LFD.Av, LFD.SD and LFD.DA recorded from each slice were calculated as a representation of the 3D microstructural distribution for each bone. Alternative 2D variables were recorded from a single mid-coronal or mid-sagittal slice of each stack for AP and LM views, respectively.¹¹

Statistical Analysis

Stepwise forward regression was used to construct mixed multiple regression models and examine the relationship between E_v and DTS parameters. Although a number of variables could be calculated from the fractal, MIL and LFD analyses, correlations

among them were expected. In order to prevent multicollinearity in the models, variation inflation factors (VIF) were examined with all potential predictors included and those causing a VIF ≥ 5 were eliminated before multiple regression analyses (see legend of Table 1).

In mixed model construction, the donor was treated as a random effect to account for pseudo-replication, E_v as the outcome variable and the set of DTS variables as the effect variables (DTS-only models). In order to examine the contribution of DTS derived variables to E_v independently from that of bone mass, the modeling process was repeated by forcing BV/TV as the first effect variable (BV/TV+DTS models). These models allowed us to examine the extent to which DTS provides information that is additional to bone mass. Separate models were constructed for different scanning orientations [axial (0°), transverse (90°), oblique (23°)] and views [AP (coronal) and LM (sagittal)] and for single-slice and stack measurements.

In order to isolate DTS variables associated with microstructure from those that are associated with the heterogeneous bone tissue mineral density, a third group of models was constructed in the same manner as above by forcing E_h as the first effect variable (E_h +DTS models). These models allowed us to examine the extent to which DTS variables contain

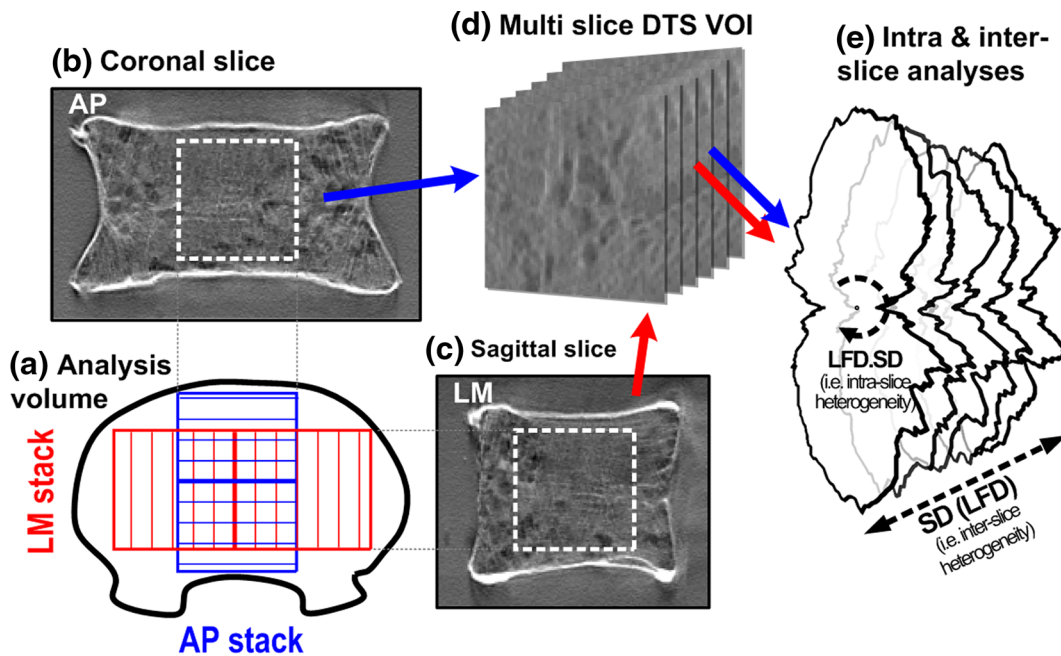


FIGURE 3. Overview of DTS analysis. (a) The regions used for the analysis of cancellous bone are illustrated by the red and blue lines for the LM and the AP image stacks, respectively. (b) Representative VOIs obtained from the coronal and (c) sagittal stacks. (d) Extracted AP and LM VOIs were analyzed slice-by-slice using LFD, MIL and fractal methods. (e) Within-slice distribution of each variable was analyzed to determine intra-slice Av , SD , Max and DA as well as inter-slice Av and SD . LFD is used as an example to illustrate the nomenclature.

tissue mineral density information relevant to cancellous bone stiffness after accounting for cancellous bone microstructure.

Mixed models that were found to be significant were rerun without the random effect to examine the extent to which aggregate data behave similarly. Paradoxical models, i.e., those in which significance of the effect is lost or the estimates changed sign, were also eliminated.

All mixed and nonmixed stepwise forward regression analyses were performed using custom scripts in JMP (v12, SAS Institute, Cary, NC).

RESULTS

Four variables calculated from a single central slice of a DTS stack and six variables calculated from the entire stack caused multicollinearity ($VIF \geq 5$) for all scan configurations and excluded from the variable set (Table 1). Additional variables calculated from the entire stack caused multicollinearity, but this depended on the DTS scan configuration (Table 1). Stack derived models were 2.9–10.7% more explanatory than the corresponding single slice derived models within the same scan configuration (Tables 2, 3). One exception was a BV/TV -included DTS model in the Axial-AP configuration where the single slice derived model was 10.3% more explanatory than the stack model.

However, only the first two predictor variables of this model were significant when the random effect was removed (Table 3).

Models constructed from Transverse scanning orientation were generally more explanatory than those from the Axial and Oblique orientations (by 2.3 and 7.5%, respectively) (Tables 2, 3). Models from Oblique scans were the least explanatory and generally were less reproducible with the aggregate data (Tables 2, 3).

Models from the LM view were more explanatory than those from the AP view (Tables 2, 3; Fig. 4). In the absence of BV/TV , stack derived models from LM view and Transverse or Axial scan orientation were comparable to BV/TV alone in their explanatory capability (R_{adj}^2 : 0.828, 0.820 and 0.816, respectively).

$Av(MIL.DA)$ and its single slice version, $MIL.DA$, were the most frequently present DTS terms in Axial and Transverse models, often partnered with additional fractal terms such as FD , S_λ and λ . Interestingly, the presence of $MIL.DA$ and $Av(MIL.DA)$ was persistent in models that contained E_n (Table 4), suggesting that these variables contain gray-level information. Contrary to all other significant DTS parameters whose estimates maintained their sign from model to model, the estimates of $MIL.DA$ variables were negative in models from the Axial orientation but positive in models from the Transverse orientation (Tables 2, 3, 4).

TABLE 1. Initial set of DTS parameters included in stepwise regression (\checkmark).

DTS parameter	Descriptions	Axial		Oblique		Transverse	
		AP	LM	AP	LM	AP	LM
Slice							
FD	Measure of complexity in graylevel texture	\checkmark	\checkmark	\checkmark	\checkmark	\checkmark	\checkmark
λ	Measure of heterogeneity in the size of holes in graylevel texture	\checkmark	\checkmark	\checkmark	\checkmark	\checkmark	\checkmark
S_λ	Slope lacunarity: rate of change in λ with size scale	\checkmark	\checkmark	\checkmark	\checkmark	\checkmark	\checkmark
LFD.Max	Measure of maximum orientation in graylevel texture	\checkmark	\checkmark	\checkmark	\checkmark	\checkmark	\checkmark
MIL.Av	Measure of avg feature size in all directions in binarized texture	\checkmark	\checkmark	\checkmark	\checkmark	\checkmark	\checkmark
MIL.DA	Anisotropy in binarized texture	\checkmark	\checkmark	\checkmark	\checkmark	\checkmark	\checkmark
LFD.DA	Anisotropy in grayvalue texture—for completeness	\checkmark	\checkmark	\checkmark	\checkmark	\checkmark	\checkmark
Stack							
Av(FD)	Interslice average of respective DTS parameters	\checkmark	\checkmark	\checkmark	\checkmark	\checkmark	\checkmark
Av(λ)		\checkmark	\checkmark	\checkmark	\checkmark	\checkmark	\checkmark
Av(S_λ)		\checkmark	\checkmark	\checkmark	\checkmark	—	—
Av(LFD.Max)		\checkmark	\checkmark	\checkmark	\checkmark	\checkmark	\checkmark
Av(MIL.Av)		\checkmark	\checkmark	\checkmark	\checkmark	\checkmark	\checkmark
Av(MIL.DA)		\checkmark	\checkmark	\checkmark	\checkmark	\checkmark	\checkmark
SD(FD)	Interslice heterogeneity of respective DTS parameters	\checkmark	\checkmark	\checkmark	\checkmark	\checkmark	\checkmark
SD(λ)		—	\checkmark	—	\checkmark	\checkmark	—
SD(S_λ)		\checkmark	\checkmark	—	—	\checkmark	\checkmark
SD(LFD.Max)		—	—	—	—	—	\checkmark
SD(MIL.DA)		—	\checkmark	—	—	—	\checkmark
SD(MIL.Av)		\checkmark	—	—	—	—	—
Av(LFD.DA)	Intersliceslice average of LFD.DA	—	—	—	\checkmark	\checkmark	\checkmark
SD(LFD.DA)	Interslice heterogeneity of respective DTS parameters	\checkmark	—	\checkmark	\checkmark	—	—
SD(LFD.Av)		—	—	\checkmark	—	—	\checkmark
SD(LFD.SD)		—	—	—	—	\checkmark	—

The dashed cells indicate that the parameter was excluded from the analysis of that scan configuration based on a multicollinearity criterion of $VIF \geq 5^*$. In addition, slice variables MIL.SD, LFD.SD, LFD.Av, MIL.Max and stack variables Av(MIL.SD), SD(MIL.SD), Av(LFD.SD), Av(LFD.Av), Av(MIL.Max), SD(MIL.Max) were excluded from all models due to their contribution to multicollinearity ($VIF \geq 5$).

*The variables were introduced in to the candidate predictor set (and presented in the table) in the order of increasing exploratory nature (Av, SD and those calculated for completeness).

DISCUSSION

The primary aim of the current study was to investigate the effects of DTS scanning orientation (with respect to the spinal axis), imaging plane and use of multiple image slices on models for predicting cancellous bone stiffness. Previous work¹¹ has demonstrated DTS derived parameters were strong correlates of μ CT derived microstructural parameters and FE stiffness in vertebral cancellous bone. The current study expanded on the previous study, which was limited to the Transverse AP configuration and analysis of single slice images, by including single and multiple slice analyses (thereby extending from 2D to 3D), AP and LM projections (coronal and sagittal), and Axial (0°), Oblique (23°) and Transverse (90°) scan orientations. In addition, in order to better simulate soft tissues, vertebral bodies were submerged in physiological saline during DTS scans. The radiopaque fixture used during scans also allowed for accurate positioning of the vertebrae with respect to the scanning geometry. The current models from the Transverse AP configuration included S_λ and Av(MIL.DA)

for the DTS-only, and MIL.DA and Av(MIL.DA) for the BV/TV + DTS models as was the case in the previous study,¹¹ while LFD.Max, LFD.SD or MIL.Av did not appear in the current models. These results suggest that S_λ and Av(MIL.DA) are relatively reproducible while the latter three are sensitive to positioning and the presence of soft tissue and thus require better control during acquisition. However, S_λ was not significant in the current study when the data were aggregated, suggesting that, despite its reproducibility, its association with bone stiffness is confounded by a stronger subject-to-subject variable.

In general, variables derived from images scanned in the Transverse orientation provided more explanatory models than those from Axial and Oblique orientations (Tables 2, 3). An exception to this was the Axial-AP case from a single slice in the presence of BV/TV (Table 3). However, when examined with the aggregate data, only one of three DTS variables in this model was significant. The model with the remaining variable was not more explanatory than the corresponding Transverse model. When used together with a measure of bone mass (BV/TV), the predictor variables were

TABLE 2. Summary of the most explanatory mixed multiple regression models of FE stiffness, constructed using DTS derived parameters alone (DTS only) from one of three scan orientations (O) and two views (V).

O	V	Slice	Stack
Axial	AP	NS	NS
	LM	0.713 (0.713)	0.820 (0.782)
		[-] MIL.Av* (0.002)	[-] Av(MIL.DA)* (0.0001)
Oblique	AP	[-] λ^* (0.008)	[-] Av(FD)* (0.0007)
		[-] FD* (0.02)	[-] Av(MIL.Av) (0.004)
	LM	RMSE = 47.4	RMSE = 38.3
Transverse	AP	NS	0.688 (NS)
			[-] Av(S_λ) (0.01)
	LM	0.627 (0.627)	RMSE = 50.0
		[-] λ^* (0.02)	0.719 (0.627)
	AP	RMSE = 53.9	[-] Av(λ)* (0.005)
		0.702 (NS)	[-] Av(FD) (0.01)
LM	[-] S_λ (0.006)	RMSE = 47.6	
	RMSE = 49.0	0.731 (0.731)	
	0.748 (NS)	[+] Av(MIL.DA)* (0.001)	
	[+] MIL.DA (0.005)	RMSE = 46.6	
	[+] LFD.Max (0.02)	0.828 (0.767)	
	RMSE = 45.1	[+] Av(MIL.DA)* (0.0007)	
		[-] SD(LFD.Av) (0.02)	
		[-] Av(FD) (0.01)	
		RMSE = 37.7	

Each cell shows R_{adj}^2 of the full model followed by the R_{adj}^2 of the reduced model containing variables that were also significant in the non-mixed model (those shown by *). [\pm] shows the sign of the estimate for each significant parameter. p values are shown in parenthesis following the variable name. RMSE = Root mean square error associated with the mixed model. NS means a statistically significant model was not found for the respective configuration.

generally more reproducible with the aggregate data for both Transverse and Axial orientations, with the Transverse models still being more explanatory. While the Transverse scan orientation appears to be preferable, there is a caveat. The geometry of the current DTS scanners is not suitable for positioning a patient perpendicular to the axis of the source–detector motion, due to the moving parts of the system. It is possible to design a system that will accommodate the Transverse scan orientation or implement the tomosynthesis algorithm in a system that has a suitable scan geometry, however, this is not yet readily available. Although slightly less explanatory than the Transverse orientation (<9%), the Axially oriented scan configuration offers a reasonable alternative as this is the default configuration in the current scanners.

Models derived from the LM view were generally more explanatory than those derived from the AP view (Tables 2, 3). This may be attributable to a larger volume of interest available for analysis in the LM view (5–17% for slice and stack, respectively), providing a more accurate assessment of the cancellous bone. It is also possible that, due to the anisotropic resolution of the DTS system, LM and AP views capture different aspects of the bone structure.²⁵ Sagittal planes are imaged in greater detail in the LM view providing a more complete sampling of the structure in the antero-posterior direction, whereas

coronal planes are imaged in greater detail in the AP view providing a more complete sampling of the structure in the lateral–medial direction. The relatively better association of the variables from the LM view with cancellous bone stiffness suggests that the organization of trabecular structure in the sagittal plane of a vertebra is important in the determination of vertebral cancellous bone stiffness. Although the AP view is most widely utilized for DTS scans in the clinical setting, there is no difficulty in positioning the patient in the DTS system for acquisition of images in the LM view, as the person simply lies down on their side in this view. Future studies should determine if additional radiation exposure is necessary and acceptable for the DTS scans with LM view.

Perhaps not too surprisingly, variables derived from the stack resulted in more explanatory models for cancellous bone stiffness than those derived from a single central slice. (*An exception is the Axial scan in AP view, as discussed above in the comparison between scan orientations.*) Morphological heterogeneity has been found to contribute cancellous bone stiffness independently from average morphology^{36,38} and it is likely that heterogeneity of bone morphology is represented better when the whole stack is utilized. However, in a majority of cases, the stack models included the “Av” rather than the “SD” of a DTS variable, suggesting that using multiple slices increases

TABLE 3. Summary of the most explanatory mixed multiple regression models of FE stiffness, constructed by forcing bone volume fraction as the first term (BV/TV + DTS) followed by DTS derived parameters from one of three scan orientations (O) and two views (V).

O	V	Slice	Stack
Axial	AP	0.915 (0.838)	0.812 (0.812)
		[+] BVTV* (0.0001)	[+] BVTV* (0.0001)
	[-] MIL.DA* (0.0007)	[-] Av(MIL.DA)* (0.02)	
	[-] S_z (0.0004)		
		RMSE = 25.7	RMSE = 35.3
	LM	0.842 (0.842)	0.912 (0.912)
		[+] BVTV* (0.0001)	[+] BVTV* (0.0001)
		[-] MIL.DA* (0.02)	[-] Av(MIL.DA)* (0.0001)
		RMSE = 33.7	[-] Av(FD)* (0.005)
			RMSE = 25.5
Oblique	AP	0.816 (0.816)	0.858 (0.816)
		[+] BVTV* (0.0001)	[+] BVTV* (0.0001)
	RMSE = 36.2	[-] Av(S_z) (0.03)	
			RMSE = 32.7
	LM	0.816 (0.816)	0.860 (0.816)
		[+] BVTV* (0.0001)	[+] BVTV* (0.0001)
		RMSE = 36.2	[-] Av(λ)* (0.01)
			[-] Av(FD) (0.03)
			RMSE = 32.0
Transverse	AP	0.874 (0.874)	0.904 (0.904)
		[+] BVTV* (0.0001)	[+] BVTV* (0.0001)
	[+] MIL.DA* (0.001)	[+] Av(MIL.DA)* (0.0001)	
	RMSE = 30.5	RMSE = 26.2	
	LM	0.893 (0.893)	0.931 (0.931)
		[+] BVTV* (0.0001)	[+] BVTV (0.0001)
		[+] MIL.DA* (0.0006)	[+] Av(MIL.DA)* (0.0001)
		[-] FD* (0.02)	[+] Av(MIL.Av)* (0.03)
		RMSE = 28.0	RMSE = 22.6

Each cell shows R_{adj}^2 of the full model followed by the R_{adj}^2 of the reduced model containing variables that were also significant in the non-mixed model (those shown by *). [\pm] shows the sign of the estimate for each significant parameter. p values are shown in parenthesis following the variable name. RMSE = Root mean square error associated with the mixed model.

the accuracy of the average measurement, rather than providing additional measures of texture heterogeneity. However, it must be noted that fractal variables, the average of which appears in the models, represent the complexity and the heterogeneity of texture. As such, it seems that heterogeneity of bone texture is captured best by measuring in separate planes (where resolution is high) and averaging over the volume (where resolution is low due to slice thickness but provides a sufficient repetition of the in-plane measurement) in a DTS system.

When variables from DTS were used alone, the success of models in predicting bone stiffness was modest compared to BV/TV alone. BV/TV was used as a reference bone density measure for cancellous bone in this study; however, it should be noted that it is only moderately correlated to clinical bone density.²⁷ The relative ability of DTS derived variables to predict stiffness of the cancellous core may be higher when compared to clinical BMD measures. Nonetheless, when used together with BV/TV, DTS derived vari-

ables contributed to cancellous bone stiffness independently from BV/TV and increased the explained variability by up to 11%. As such, DTS appears suitable for complementing bone mass measurements.

A persistent presence of MIL.DA (single slice or stack average) was noted in the models, especially when used together with BV/TV. MIL.DA is the ratio of two principal MILs and represents the degree of anisotropy in the image pattern. Degree of anisotropy is a well-known morphological parameter associated with mechanical properties of cancellous bone.^{9,17,31,39} More recently, it was reported that BV/TV and fabric anisotropy, a form of anisotropy derived from MILs, are two most important predictors of human cancellous bone stiffness.¹⁶ It was reported that anisotropy explains approximately an additional 10% in cancellous bone stiffness beyond BV/TV in that μ CT study, coincidentally mirroring the finding of the current study.

Interestingly, MIL.DA (single slice or stack average) was significant in stiffness models in which stiff-

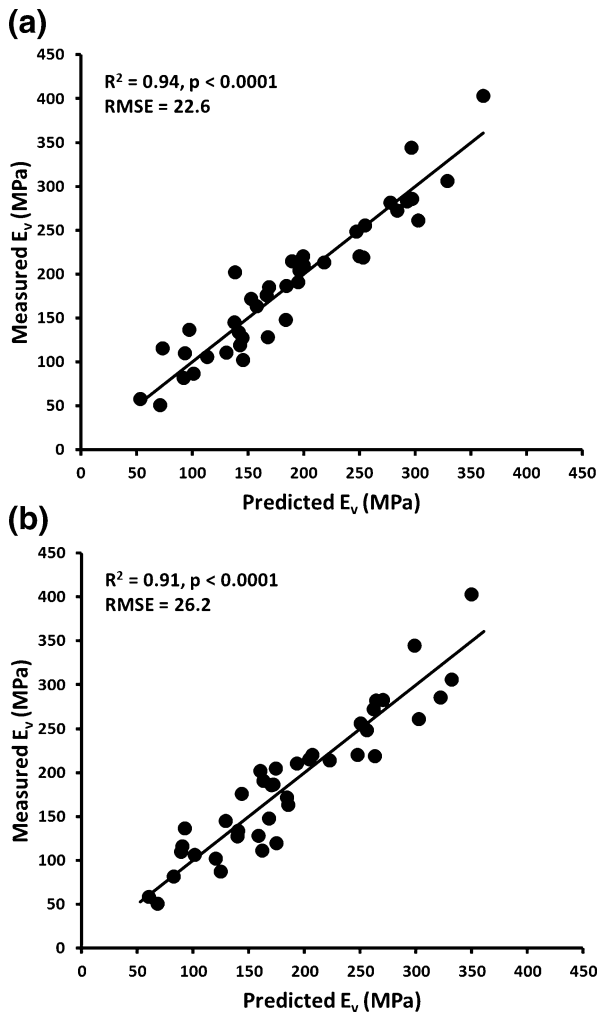


FIGURE 4. (a) Measured vs predicted E_v using the image stack from the transverse orientation in LM view ($E_v = 1676 \text{ BV/TV} + 14 \text{ Av(MIL.Av)} + 293 \text{ Av(MIL.DA)} - 583$). (b) Measured vs predicted E_v using the image stack from the transverse orientation in AP view ($E_v = 1730 \text{ BV/TV} + 283 \text{ Av(MIL.DA)} - 502$). For illustration of prediction error, the identity line (solid) and the root mean square error (RMSE) are shown.

ness from homogenous models were forced. Considering that the homogenous models should account for all the microstructural information, this result suggests that MIL.DA contains information, albeit small, on the gray level distribution within the structure and possibly on the bone material. Since MIL.DA is calculated from binarized images, it is not a gray level parameter per se, but it can be affected by the intensity distributions during the binarization process. In order to illustrate this effect, we simulated cancellous bone with fixed trabecular microstructure but with increasing levels of gray values representing increasing levels of trabecular tissue mineralization, together with a fixed level of Gaussian noise (Fig. 5). Application of the MIL procedures to the simulated images indicated

TABLE 4. Summary of the mixed multiple regression models of heterogeneous FE stiffness for three DTS scan orientations (O) and two views (V), with homogeneous FE stiffness (E_h) forced as the first term so as to isolate microstructure from material level information.

O	V	Slice	Stack	
Axial	AP	0.980	0.983 [+] E_h^* (0.0001)	
		[+] E_h^* (0.0001) [-] MIL.DA* (0.04)	[-] Av(MIL.DA)* (0.008) [-] Av(S_z) (0.02)	
	LM	0.981	0.980	
		[+] E_h^* (0.0001) [-] MIL.DA (0.03)	[+] E_h^* (0.0001) [-] Av(MIL.DA)* (0.02)	
	Oblique	AP	0.978	0.981
			[+] E_h^* (0.0001)	[+] E_h^* (0.0001) [-] Av(S_z) (0.04)
LM		0.978	0.982	
		[+] E_h^* (0.0001)	[+] E_h^* (0.0001) [+] Av(MIL.DA)* (0.02) [-] SD(FD) (0.02)	
Transverse	AP	0.986	0.987	
		[+] E_h^* (0.0001) [+] MIL.DA* (0.02)	[+] E_h^* (0.0001)	
		[-] S_z (0.03)	[+] Av(MIL.DA)* (0.0001)	
		LM	0.986	0.989
	LM	[+] E_h^* (0.0001) [+] MIL.DA* (0.0001)	[+] E_h^* (0.0001) [+] Av(MIL.DA)* (0.0001)	

Each cell shows R_{adj}^2 of the model followed by the significant effect variable. [±] shows the sign of the estimate for each significant parameter. p values are shown in parenthesis following the variable name. Effect variables that remained significant in the matching non-mixed models are also shown (*).

that increasing bone to background contrast with increasing levels of mineralization affects the segmentation and binarization of the image, which subsequently resulted in an increase in MIL.DA. As such, MIL.DA appears to represent the level of mineralization, in addition to structural information, in this analysis. Alternatively, MIL.DA may be correlated to another property of the tissue that affects stiffness, but not examined in the current study. If true, biological mechanisms underlying such correlation would be of interest in future studies.

Although MIL.DA (slice or stack average) was consistently present in the models, it was also the only DTS parameter whose sign was different between Transverse and Axial models (Tables 2, 3). Because MIL.DA is calculated as the ratio of the first and the third principal MIL values, this cannot be explained simply by how the coordinate system is set in a given plane. However, it may be attributable to the orientation dependent sensitivity of the DTS system²⁴ (Fig. 2), meaning that increasing MIL.DA may indicate increased orientation in the SI direction for Transverse scans but increased orientation in the transverse directions for Axial scans. This is more so if bone mass is fixed, i.e., more orientation in one direc-

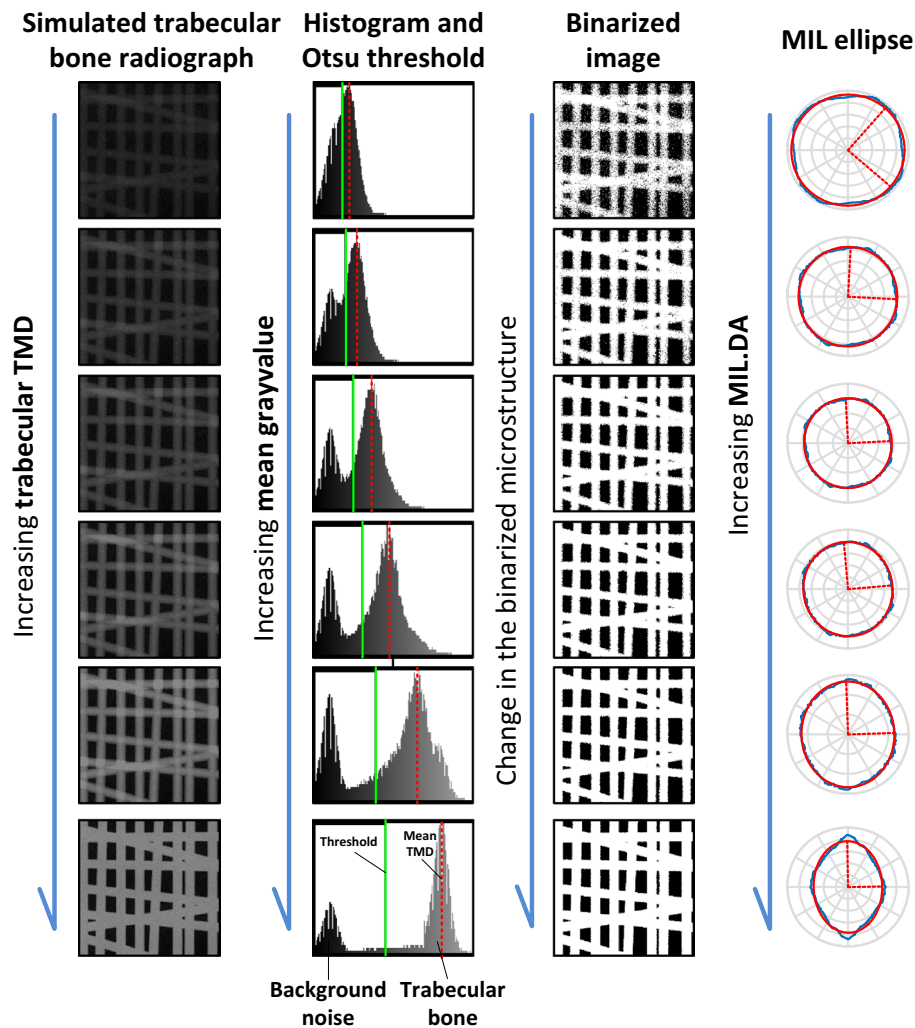


FIGURE 5. Simulation to illustrate the potential effect of tissue mineral density (TMD) on the binarization of a 2D projection and, subsequently, on the calculated MIL anisotropy. The underlying microstructure was kept constant while the gray level was varied. As the simulated TMD increased the binarized images became more anisotropic or, conversely, anisotropy is reduced with increasing overlap between background and bone graylevels.

tion would be associated with lack of orientation in other directions. Because increasing uniaxial stiffness of cancellous bone would be largely associated with increased orientation of trabeculae in the SI direction, measurements of MIL.DA from both Axial and Transverse scans could correlate with stiffness but with a different sign. However, this remains a speculation to be substantiated in future studies.

The limitations of the current study include its exploratory approach in the construction of the predictive models. Commonly, MIL is used to derive an average value (representing feature thickness) or calculate anisotropy while LFD is used to calculate a maximum value representing orientation. Both methods calculate variables in various directions in the plane of analysis, giving a distribution of values for

each plane. In an attempt to capture additional information from each distribution and to calculate comparable variables between analyses, we included additional variables (such as MIL.Max and LFD.DA) in the set. In addition, the methods of MIL, LFD and fractal analysis have been used previously but typically with single images such as from a radiogram. Our utilization of a stack introduced additional variables that represent the slice to slice heterogeneity in the texture (SD variables), further increasing the number of candidate predictor variables. By using VIFs and comparing mixed model results to those from aggregate data, we eliminated the paradoxical models and those with multicollinearity. However, further verification may be necessary by use of an independent set of data in future work.

The current study was focused on a portion of the cancellous bone within a vertebra rather than the whole vertebra. However, this was a necessary step as the image analysis methods used in the current study are for examining cancellous bone texture alone. Once the capability of DTS to characterize cancellous bone is determined, additional approaches can be built on this foundation to extend DTS based techniques to cover whole vertebrae.

Finite element calculated cancellous bone stiffness, rather than experimentally determined strength, was used as the primary outcome. The computational nature of the work allowed us to study cancellous microstructure in isolation. This way, the vertebrae were left intact for future whole vertebra mechanical studies. Considering that human vertebral cancellous bone stiffness and strength are strongly correlated¹⁰ and that large scale FE calculation of cancellous bone stiffness is highly accurate,² the use of FE stiffness in the current study is reasonable for the stated advantages.

In summary, we examined three scanning directions (Axial, Oblique, Perpendicular) in two views (AP, LM), giving a total of six DTS configurations and the use of slice (2D) and stack (3D) images from each configuration for the most explanatory models predicting FE stiffness of vertebral cancellous bone. In general, models associated with the Transverse scanning orientation and the LM view utilizing stack parameters provided more explanatory models than their respective alternatives. DTS derived variables increased explained variability in cancellous bone stiffness by up to 11.5% beyond that explained by BV/TV alone. MIL.DA frequently appeared in the models and possibly provided material in addition to microstructural information. The current results are expected to inform future studies aiming at improving the assessment of vertebral bone quality and fracture risk in the clinical environment.

ACKNOWLEDGMENTS

This project was supported, in part, by the National Institutes of Health under Grant Number AR059329 and by the Department of Defense Peer Reviewed Medical Research Program, under Award Number W81XWH-11-1-0769. Views and opinions of, and endorsements by the authors do not reflect those of the US Army or the Department of Defense or those of the NIH. Human tissue used in the presented work was provided by NDRI (National Disease Research Interchange).

CONFLICT OF INTEREST

No benefits in any form have been or will be received from a commercial party related directly or indirectly to the subject of this manuscript.

REFERENCES

- ¹Bauer, J. S., S. Kohlmann, F. Eckstein, D. Mueller, E. M. Lochmuller, and T. M. Link. Structural analysis of trabecular bone of the proximal femur using multislice computed tomography: a comparison with dual X-ray absorptiometry for predicting biomechanical strength in vitro. *Calcif Tissue Int* 78:78–89, 2006.
- ²Chevalier, Y., D. Pahr, H. Allmer, M. Charlebois, and P. Zysset. Validation of a voxel-based FE method for prediction of the uniaxial apparent modulus of human trabecular bone using macroscopic mechanical tests and nanoindentation. *J Biomech* 40:3333–3340, 2007.
- ³Eckstein, F., M. Fischbeck, V. Kuhn, T. M. Link, M. Priemel, and E. M. Lochmuller. Determinants and heterogeneity of mechanical competence throughout the thoracolumbar spine of elderly women and men. *Bone* 35:364–374, 2004.
- ⁴Fazzalari, N. L., and I. H. Parkinson. Fractal dimension and architecture of trabecular bone. *J Pathol* 178:100–105, 1996.
- ⁵Fields, A. J., S. K. Eswaran, M. G. Jekir, and T. M. Keaveny. Role of trabecular microarchitecture in whole-vertebral body biomechanical behavior. *J Bone Miner Res* 24:1523–1530, 2009.
- ⁶Flynn, M. J., R. McGee, and J. Blechinger. Spatial Resolution of X-ray Tomosynthesis in Relation to Computed Tomography for Coronal/Sagittal Images of the Knee (PART 1 ed.). San Diego: SPIE, p. 65100D-9, 2007.
- ⁷Gazaille, 3rd, R. E., M. J. Flynn, W. Page, 3rd, S. Finley, and M. van Holsbeeck. Technical innovation: digital tomosynthesis of the hip following intra-articular administration of contrast. *Skelet. Radiol.* 40:1467–1471, 2011.
- ⁸Geraets, W. G. Comparison of two methods for measuring orientation. *Bone* 23:383–388, 1998.
- ⁹Hodgskinson, R., and J. D. Currey. The effect of variation in structure on the Young's modulus of cancellous bone: a comparison of human and non-human material. *Proc. Inst. Mech. Eng. H* 204:115–121, 1990.
- ¹⁰Hou, F. J., S. M. Lang, S. J. Hoshaw, D. A. Reimann, and D. P. Fyhrie. Human vertebral body apparent and hard tissue stiffness. *J. Biomech.* 31:1009–1015, 1998.
- ¹¹Kim, W., D. Oravec, S. Nekkanty, J. Yerramshetty, E. A. Sander, G. W. Divine, M. J. Flynn, and Y. N. Yeni. Digital tomosynthesis (DTS) for quantitative assessment of trabecular microstructure in human vertebral bone. *Med. Eng. Phys.* 37:109–120, 2015.
- ¹²Krug, R., J. Carballido-Gamio, A. J. Burghardt, G. Kazakia, B. H. Hyun, B. Jobke, S. Banerjee, M. Huber, T. M. Link, and S. Majumdar. Assessment of trabecular bone structure comparing magnetic resonance imaging at 3 Tesla with high-resolution peripheral quantitative computed tomography ex vivo and in vivo. *Osteoporos. Int.* 19:653–661, 2008.
- ¹³Kuhn, J. L., S. A. Goldstein, L. A. Feldkamp, R. W. Goulet, and G. Jesion. Evaluation of a microcomputed

- tomography system to study trabecular bone structure. *J. Orthop. Res.* 8:833–842, 1990.
- ¹⁴Liu, X. S., X. H. Zhang, K. K. Sekhon, M. F. Adams, D. J. McMahon, J. P. Bilezikian, E. Shane, and X. E. Guo. High-resolution peripheral quantitative computed tomography can assess microstructural and mechanical properties of human distal tibial bone. *J. Bone Miner. Res.* 25:746–756, 2010.
 - ¹⁵Majumdar, S., T. M. Link, P. Augat, J. C. Lin, D. Newitt, N. E. Lane, and H. K. Genant. Trabecular bone architecture in the distal radius using magnetic resonance imaging in subjects with fractures of the proximal femur. Magnetic Resonance Science Center and Osteoporosis and Arthritis Research Group. *Osteoporos. Int.* 10:231–239, 1999.
 - ¹⁶Maquer, G., S. N. Musy, J. Wandel, T. Gross, and P. K. Zysset. Bone volume fraction and fabric anisotropy are better determinants of trabecular bone stiffness than other morphological variables. *J. Bone Miner. Res.* 30:1000–1008, 2015.
 - ¹⁷Matsuura, M., F. Eckstein, E. M. Lochmuller, and P. K. Zysset. The role of fabric in the quasi-static compressive mechanical properties of human trabecular bone from various anatomical locations. *Biomech. Model. Mechanobiol.* 7:27–42, 2008.
 - ¹⁸McBroom, R. J., W. C. Hayes, W. T. Edwards, R. P. Goldberg, and A. A. White, 3rd. Prediction of vertebral body compressive fracture using quantitative computed tomography. *J. Bone Joint Surg. Am.* 67:1206–1214, 1985.
 - ¹⁹Mosekilde, L., S. M. Bentzen, G. Ortoft, and J. Jorgensen. The predictive value of quantitative computed tomography for vertebral body compressive strength and ash density. *Bone* 10:465–470, 1989.
 - ²⁰Nazarian, A., M. Stauber, D. Zurakowski, B. D. Snyder, and R. Muller. The interaction of microstructure and volume fraction in predicting failure in cancellous bone. *Bone* 39:1196–1202, 2006.
 - ²¹Nekkanty, S., J. Yerramshetty, D. G. Kim, R. Zauel, E. Johnson, D. D. Cody, and Y. N. Yeni. Stiffness of the endplate boundary layer and endplate surface topography are associated with brittleness of human whole vertebral bodies. *Bone* 47:783–789, 2010.
 - ²²Nevitt, M. C., P. D. Ross, L. Palermo, T. Musliner, H. K. Genant, and D. E. Thompson. Association of prevalent vertebral fractures, bone density, and alendronate treatment with incident vertebral fractures: effect of number and spinal location of fractures. The Fracture Intervention Trial Research Group. *Bone* 25:613–619, 1999.
 - ²³Newitt, D. C., S. Majumdar, B. van Rietbergen, G. von Ingersleben, S. T. Harris, H. K. Genant, C. Chesnut, P. Garnero, and B. MacDonald. In vivo assessment of architecture and micro-finite element analysis derived indices of mechanical properties of trabecular bone in the radius. *Osteoporos. Int.* 13:6–17, 2002.
 - ²⁴Notohara, D., K. Nishino, and K. Shibata. First Physical Measurements and Clinical Evaluation for Long-View Tomosynthesis. In: SPIE, edited by E. Samei and J. Hsieh, 72581K-9, 2009.
 - ²⁵Oravec, D., A. Quazi, A. Xiao, E. Yang, R. Zauel, M. J. Flynn, and Y. N. Yeni. Digital tomosynthesis and high resolution computed tomography as clinical tools for vertebral endplate topography measurements: comparison with microcomputed tomography. *Bone* 81:300–305, 2015.
 - ²⁶Ortoft, G., L. Mosekilde, C. Hasling, and L. Mosekilde. Estimation of vertebral body strength by dual photon absorptiometry in elderly individuals: comparison between measurements of total vertebral and vertebral body bone mineral. *Bone* 14:667–673, 1993.
 - ²⁷Perilli, E., A. M. Briggs, S. Kantor, J. Codrington, J. D. Wark, I. H. Parkinson, and N. L. Fazzalari. Failure strength of human vertebrae: prediction using bone mineral density measured by DXA and bone volume by micro-CT. *Bone* 50:1416–1425, 2012.
 - ²⁸Plotnick, R. E., R. H. Gardner, W. W. Hargrove, K. Prestegard, and M. Perlmuter. Lacunarity analysis: a general technique for the analysis of spatial patterns. *Phys. Rev. E* 53:5461–5468, 1996.
 - ²⁹Reimann, D. A., S. M. Hames, M. J. Flynn, and D. P. Fyhrie. A cone beam computed tomography system for true 3D imaging of specimens. *Appl. Radiat. Isot.* 48:1433–1436, 1997.
 - ³⁰Tabensky, A. D., J. Williams, V. DeLuca, E. Briganti, and E. Seeman. Bone mass, areal, and volumetric bone density are equally accurate, sensitive, and specific surrogates of the breaking strength of the vertebral body: an in vitro study. *J. Bone Miner. Res.* 11:1981–1988, 1996.
 - ³¹Turner, C. H. On Wolff's Law of trabecular architecture. *J. Biomech.* 25:1–9, 1992.
 - ³²Ulrich, D., B. van Rietbergen, A. Laib, and P. Rueggsegger. The ability of three-dimensional structural indices to reflect mechanical aspects of trabecular bone. *Bone* 25:55–60, 1999.
 - ³³Wehrli, F. W., B. R. Gomberg, P. K. Saha, H. K. Song, S. N. Hwang, and P. J. Snyder. Digital topological analysis of in vivo magnetic resonance microimages of trabecular bone reveals structural implications of osteoporosis. *J. Bone Miner. Res.* 16:1520–1531, 2001.
 - ³⁴Whitehouse, W. J. The quantitative morphology of anisotropic trabecular bone. *J. Microsc.* 101(Pt 2):153–168, 1974.
 - ³⁵Wright, N. C., A. C. Looker, K. G. Saag, J. R. Curtis, E. S. Delzell, S. Randall, and B. Dawson-Hughes. The recent prevalence of osteoporosis and low bone mass in the United States based on bone mineral density at the femoral neck or lumbar spine. *J. Bone Miner. Res.* 29:2520–2526, 2014.
 - ³⁶Yeh, O. C., and T. M. Keaveny. Biomechanical effects of intraspecimen variations in trabecular architecture: a three-dimensional finite element study. *Bone* 25:223–228, 1999.
 - ³⁷Yeni, Y. N., and D. P. Fyhrie. Finite element calculated uniaxial apparent stiffness is a consistent predictor of uniaxial apparent strength in human vertebral cancellous bone tested with different boundary conditions. *J. Biomech.* 34:1649–1654, 2001.
 - ³⁸Yeni, Y. N., M. J. Zinno, J. S. Yerramshetty, R. Zauel, and D. P. Fyhrie. Variability of trabecular microstructure is age-, gender-, race- and anatomic site-dependent and affects stiffness and stress distribution properties of human vertebral cancellous bone. *Bone* 49:886–894, 2011.
 - ³⁹Zysset, P. K., R. W. Goulet, and S. J. Hollister. A global relationship between trabecular bone morphology and homogenized elastic properties. *J. Biomech. Eng.* 120:640–646, 1998.